Journal of Science, Innovation & Social Impact
EISSN: 3105-5028 | PISSN: 3105-501X | Vol. 2, No. 1 (2026)

Article

Multi-Objective Optimization of Process Parameters for Dental Resin 3D Printing Using Improved NSGA-II Algorithm

Pei-Ting Chung [1,*]

[1] Chemical and Biomolecular Engineering, University of California Irvine, CA, USA
* Correspondence: Pei-Ting Chung, Chemical and Biomolecular Engineering, University of California Irvine, CA, USA

Abstract: This study presents an improved Non-dominated Sorting Genetic Algorithm II (NSGA-II) for optimizing process parameters in dental resin 3D printing. The optimization framework addresses three conflicting objectives: dimensional accuracy, surface roughness, and printing time. Five critical process parameters, including layer thickness, exposure duration, print angle, infill density, and lift speed, are investigated using a design of experiments approach based on Response Surface Methodology. The improved NSGA-II incorporates an adaptive mutation operator and an elite-preservation strategy to enhance convergence and solution diversity. Experimental validation using nine dental model resin types demonstrates that the proposed algorithm achieves a 25.3% improvement in dimensional accuracy compared to default parameter settings. The Pareto-optimal solutions provide dental laboratories with flexible parameter configurations that balance quality requirements and production efficiency. Statistical analysis confirms that layer thickness and exposure duration are the most influential parameters affecting print quality.

Keywords: multi-objective optimization; NSGA-II; dental resin; 3D printing parameters

1. Introduction

1.1. Background and Motivation

1.1.1. Development of 3D Printing Technology in Dental Applications

Three-dimensional printing technology has revolutionized dental manufacturing by enabling rapid fabrication of customized prosthetics, aligners, and surgical guides. Digital Light Processing (DLP) and Stereolithography (SLA) represent the predominant photopolymerization-based additive manufacturing techniques employed in contemporary dental laboratories. These technologies cure photosensitive resin layer by layer through controlled light exposure, producing dental appliances with high geometric complexity and fine surface details. The global dental 3D printing market has experienced substantial growth, driven by increasing demand for personalized dental treatments and the integration of digital workflows in clinical practice [1].

The transition from conventional to additive manufacturing in dentistry offers significant advantages in design flexibility, material efficiency, and production speed. Resin-based 3D printing enables the fabrication of dental crowns, bridges, denture bases, and orthodontic models with dimensional tolerances approaching clinical requirements. The layer-by-layer fabrication approach eliminates tooling constraints inherent to subtractive manufacturing while reducing material waste by up to 40% compared to milling processes [2].

Received: 18 January 2026
Revised: 28 February 2026
Accepted: 12 March 2026
Published: 18 March 2026

Copyright: © 2026 by the authors. Submitted for possible open access publication under the terms and conditions of the Creative Commons Attribution (CC BY) license (https://creativecommons.org/licenses/by/4.0/).

1.1.2. Challenges in Parameter Optimization for Dental Resin Printing

Despite technological advances, achieving consistent print quality remains challenging due to the complex interdependencies among process parameters. Layer thickness, exposure time, print orientation, and post-curing conditions interact nonlinearly to influence dimensional accuracy, surface finish, and mechanical properties of printed parts [3]. Dental applications impose stringent quality requirements, with marginal gaps exceeding 50 micrometers potentially compromising restoration longevity and clinical outcomes.

The parameter optimization problem becomes particularly complex when multiple quality attributes must be simultaneously optimized. Improving dimensional accuracy often requires thinner layers and longer exposure times, which increase production duration and energy consumption. This inherent trade-off between quality and efficiency necessitates multi-objective optimization approaches capable of identifying Pareto-optimal parameter configurations [4].

1.2. Research Objectives and Scope

1.2.1. Problem Statement

This research addresses the multi-objective parameter-optimization problem in dental resin 3D printing. The objective is to minimize dimensional deviation, surface roughness, and printing time simultaneously while respecting process constraints.

1.2.2. Research Questions

The study investigates: (1) How do individual process parameters and their interactions affect print quality metrics? (2) Can an improved NSGA-II algorithm effectively generate Pareto-optimal parameter configurations? (3) What parameter sensitivity patterns exist across different dental resin formulations?

1.2.3. Contribution of This Study

This work contributes an enhanced NSGA-II algorithm incorporating adaptive operators specifically designed for the dental resin printing optimization problem. The research provides quantitative guidelines for parameter selection and demonstrates algorithm effectiveness through comprehensive experimental validation.

1.3. Paper Organization

Section 2 reviews relevant literature on 3D printing optimization and evolutionary algorithms. Section 3 details the proposed methodology, including problem formulation and algorithm design. Section 4 presents experimental results and comparative analysis. Section 5 concludes with findings and future research directions.

2. Literature Review

2.1. 3D Printing Technologies for Dental Applications

2.1.1. DLP and SLA Printing Principles

Digital Light Processing technology projects entire-layer images onto photosensitive resin using digital micromirror devices, enabling rapid curing of entire cross-sections. The projection-based approach offers speed advantages over laser-scanning SLA systems while maintaining high resolution capabilities. Contemporary DLP printers achieve XY resolutions of 25-50 micrometers with layer thicknesses ranging from 25 to 100 micrometers [5]. The photopolymerization reaction involves radical-initiated chain-growth polymerization of acrylate monomers, with reaction kinetics governed by light intensity, photoinitiator concentration, and exposure duration.

SLA technology uses focused ultraviolet laser beams to trace and sequentially solidify resin patterns. The vector-based scanning approach provides consistent energy delivery across the build platform but requires longer processing times for large cross-

sectional areas [6]. Both technologies require careful calibration of exposure parameters to achieve optimal cure depth and minimize overcuring or undercuring defects.

2.1.2. Key Process Parameters in Resin Printing

Layer thickness directly influences surface roughness through stair-stepping effects and affects dimensional accuracy through cure-depth variations [7]. Exposure duration controls the extent of polymerization and the interlayer adhesion strength. Print orientation determines support structure requirements and influences anisotropic mechanical properties. Lift speed and separation distance affect peeling forces during layer transitions, particularly critical for large cross-sectional areas.

2.2. Multi-Objective Optimization Methods

2.2.1. Evolutionary Algorithms for Parameter Optimization

Evolutionary algorithms have demonstrated effectiveness for manufacturing parameter optimization due to their population-based search capabilities and gradient-free operation. Genetic algorithms, particle swarm optimization, and differential evolution have been successfully applied to the optimization of additive manufacturing processes [8]. These metaheuristic approaches handle nonlinear objective functions and discrete parameter spaces common in manufacturing applications.

2.2.2. NSGA-II and Its Variants

The Non-dominated Sorting Genetic Algorithm II is a benchmark multi-objective evolutionary algorithm characterized by fast non-dominated sorting and crowding-distance-based diversity preservation [9]. NSGA-II efficiently generates well-distributed Pareto fronts through elitist selection mechanisms. Recent variants incorporate adaptive operator control, reference-point guidance, and archive strategies to improve convergence in high-dimensional objective spaces.

2.2.3. Hybrid Optimization Approaches

Hybrid methods combining evolutionary algorithms with response surface models or machine learning surrogates have gained attention for computationally expensive optimization problems [10]. Bayesian optimization approaches guide experimental sampling toward promising parameter regions, reducing the number of physical experiments required for optimization.

2.3. Parameter Sensitivity Analysis Methods

2.3.1. Design of Experiments Approaches

Taguchi methods provide an efficient way to screen significant factors using orthogonal arrays, reducing the experimental burden compared to full factorial designs. The signal-to-noise ratio formulation enables robust parameter selection that minimizes output variability [11]. Central composite and Box-Behnken designs support response surface model fitting for quantifying parameter effects and interactions.

2.3.2. Response Surface Methodology

Response Surface Methodology constructs polynomial regression models relating process parameters to output responses, where factors are fitted in coded form and then mapped back to physical units for interpretation. Second-order models capture curvature and interaction effects, which are essential for optimization near response optima [12]. The methodology enables the prediction of responses at untested parameter combinations and the identification of stationary points through gradient analysis.

3. Methodology

3.1. Problem Formulation

3.1.1. Definition of Optimization Objectives

The multi-objective optimization problem addresses three competing objectives: dimensional accuracy f1(x) measured as root mean square deviation between printed specimens and CAD specifications, surface roughness f2(x) quantified using arithmetic mean deviation Ra perpendicular to build direction, and printing time f3(x) including layer exposure and platform movement operations.

The mathematical formulation is expressed as:

Minimize F(x) = [f1(x), f2(x), f3(x)]

Subject to: xL <= x <= xU

Where x = [x1, x2, x3, x4, x5] represents the decision variable vector containing layer thickness, exposure duration, print angle, infill density, and lift speed.

Table 1 presents the decision variables, their corresponding ranges, and the units used in this optimization study.

Table 1. Process Parameter Ranges for Optimization.

Parameter	Symbol	Lower Bound	Upper Bound	Unit
Layer Thickness	x1	25	100	μm
Exposure Duration	x2	1.5	8.0	s
Print Angle	x3	0	90	degree
Infill Density	x4	50	100	%
Lift Speed	x5	30	150	mm/min

3.1.2. Parameter Space and Constraints

The parameter space comprises 5 continuous decision variables spanning the practical operating ranges of DLP-based dental resin printers. Layer thicknesses below 25 micrometers exceed typical projector resolution, while those exceeding 100 micrometers produce unacceptable surface quality for dental applications. Exposure duration ranges reflect manufacturer recommendations for dental model resins with standard photoinitiator concentrations [13].

Constraint functions ensure printed specimens satisfy minimum mechanical property requirements. The flexural strength constraint requires printed samples to exceed 45 MPa (with 50 MPa treated as a practical target for temporary dental restorations, depending on resin formulation). The degree of conversion constraint mandates polymerization levels above 70% to prevent cytotoxicity concerns from residual monomer. These constraints are handled via penalty functions within the optimization algorithm.

3.2. Proposed Optimization Framework

3.2.1. Improved NSGA-II Algorithm Design

The proposed Improved NSGA-II (I-NSGA-II) algorithm incorporates three enhancements over the standard implementation. The first enhancement involves an adaptive crossover probability that adjusts recombination rates based on population diversity metrics. The adaptive crossover probability is computed as:

Pc = Pc_min + (Pc_max - Pc_min) * (1 - CD_var / CD_max)

Where Pc_min and Pc_max represent minimum and maximum crossover probabilities set to 0.6 and 0.95, CD_var denotes current population crowding distance variance, and CD_max represents maximum observed variance. The second enhancement implements polynomial mutation with a self-adaptive distribution index that is updated each generation based on population diversity (crowding-distance variance). The distribution index eta controls mutation step sizes, with larger values producing smaller perturbations [14].

The third enhancement incorporates an external archive with size management for preserving high-quality non-dominated solutions. Archive solutions participate in tournament selection with probability Pa = 0.3.

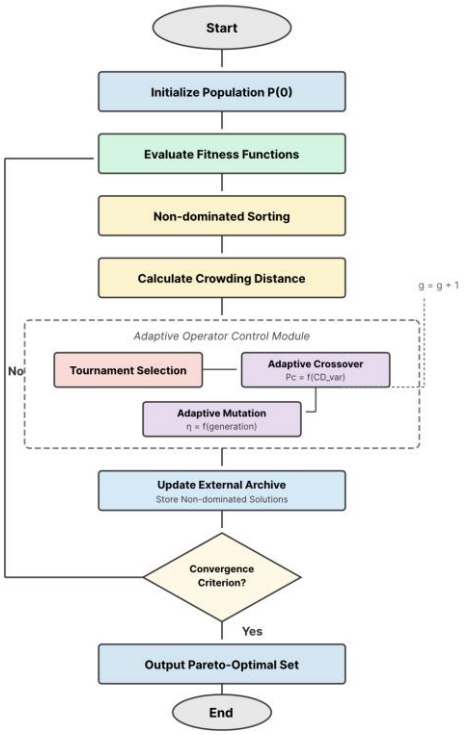

Figure 1. Flowchart of the Improved NSGA-II Algorithm.

The figure illustrates the complete algorithmic workflow of the proposed I-NSGA-II optimization framework. The flowchart begins with random population initialization within the defined parameter bounds, proceeding through iterative cycles of fitness evaluation, non-dominated sorting, crowding distance calculation, and genetic operations. The adaptive operator control module monitors population diversity metrics and adjusts crossover probability and mutation distribution index accordingly. External archive update operations occur after each generation, removing dominated solutions and applying size-limiting truncation when archive capacity is exceeded. Convergence detection based on hypervolume indicator stability determines algorithm termination. Decision paths for constraint handling, archive management, and adaptive parameter updates are clearly delineated through conditional branching.

3.2.2. Fitness Function Construction

The fitness evaluation integrates experimental measurements with surrogate model predictions. Response surface models fitted to initial experimental data provide rapid fitness approximations during evolutionary search. The fitness assignment employs non-dominated ranking, where solutions in the first front receive rank 1. Within each front, crowding distance quantifies solution density in objective space. Table 2 provides an excerpt of the Response Surface Methodology experimental design matrix based on a Central Composite Design (CCD); the complete 32-run CCD matrix is provided in the supplementary materials.

Table 2. Excerpt of the Central Composite Design Matrix and Experimental Responses.

Run	x1 (μm)	x2 (s)	x3 (°)	x4 (%)	x5 (mm/min)	f1 (μm)	f2 (μm)	f3 (min)
1	50	3.5	30	75	90	42.3	3.21	28.5
2	25	2.0	15	60	60	31.5	2.45	52.3
3	75	5.0	45	90	120	58.7	4.12	18.7

4	100	6.5	60	85	150	72.4	5.34	14.2
5	50	4.5	45	75	90	38.9	3.05	31.2
6	37	3.0	22	68	75	35.2	2.78	41.8
7	62	4.0	38	82	105	48.6	3.56	24.6
8	50	3.5	30	75	90	43.1	3.18	28.9

Note: The complete 32-run CCD matrix is available in the supplementary materials.

3.2.3. Constraint Handling Mechanism

The constraint handling employs a penalty function that degrades the fitness values of infeasible solutions in proportion to the magnitude of the constraint violation. The penalty function is formulated as:

P(x) = sum (max(0, gj(x))^2) for j = 1 to m

Where gj(x) represents the jth constraint function, normalized to yield positive values for violations.

3.3. Experimental Design

3.3.1. Parameter Selection and Ranges

Parameter ranges were established through preliminary screening experiments and equipment manufacturer specifications. Layer thickness is the most influential parameter affecting both surface quality and production speed, according to prior sensitivity analyses. The selected range of 25-100 micrometers spans typical dental printing applications, from high-precision crown margins to rapid-prototyping models [15].

Exposure duration interacts strongly with layer thickness and resin composition. Dental model resins containing camphorquinone photoinitiator systems typically require 2-6 seconds of exposure per layer at standard DLP projector intensities of 10-15 mW/cm2. Extended exposure compensates for light attenuation in pigmented resins, but it also risks overcuring artifacts.

Table 3 summarizes the resin materials evaluated in experimental validation along with manufacturer-specified viscosity and reactivity characteristics.

Table 3. Dental Resin Materials and Properties.

Resin Type	Manufacturer	Viscosity *mPa·s*	Recommended Layer (μm)	Flexural Strength (MPa)
Model Resin V2	FormLabs	850	50	61.5
Dental Model	NextDent	1200	50	58.2
KeyModel Ultra	Keystone	750	25-50	72.4
DETAX Model	DETAX	920	50	65.8
SprintRay Model	SprintRay	680	50-100	55.3
Asiga DentaMODEL	Asiga	780	50	68.9
Shining Model	Shining3D	890	50	59.7
Phrozen Aqua	Phrozen	45	50	52.1
Anycubic Grey	Anycubic	150	50	48.6

3.3.2. Response Variables Definition

Three response variables quantify printed specimen quality and production performance. Dimensional accuracy is assessed by measuring standardized test specimens using a coordinate measuring machine with 2-micrometer resolution. Measurements are taken at 12 predefined datum points on each specimen, with root mean square deviation computed against nominal CAD dimensions.

Surface roughness is measured using a stylus profilometer with a 2-micrometer tip radius traversing 4-millimeter evaluation lengths perpendicular to layer lines. The arithmetic mean deviation Ra is computed according to ISO 4287 standards from five repeated measurements per specimen.

4. Experimental Results and Discussion

4.1. Experimental Setup

4.1.1. Materials and Equipment

Experiments were conducted using a Phrozen Sonic Mini 8K DLP printer with 22-micrometer XY resolution and 405-nanometer LED light source. Nine dental model resin formulations representing major market segments were evaluated. Specimens were printed in batches of 6 units per build platform. Post-processing included 3-minute isopropanol wash cycles followed by 60-second UV post-curing at 50°C. Dimensional measurements were performed using a Zeiss CONTURA coordinate measuring machine with a probing uncertainty of 1.8 micrometers. Surface roughness was characterized using a Mitutoyo SJ-410 stylus profilometer.

4.1.2. Evaluation Metrics

Algorithm performance was assessed using hypervolume indicator, generational distance, and inverted generational distance metrics. Hypervolume quantifies the volume of the objective space dominated by the obtained Pareto front. The reference point for hypervolume calculation was set to [100, 8, 60]. Statistical significance was assessed using the Wilcoxon rank-sum test at the 0.05 significance level.

4.2. Algorithm Performance Analysis

4.2.1. Convergence Analysis

The improved NSGA-II algorithm demonstrated stable convergence across 30 independent runs. The hypervolume indicator reached 95% of final values within 150 generations. The adaptive operator control mechanism effectively balanced exploration and exploitation phases.

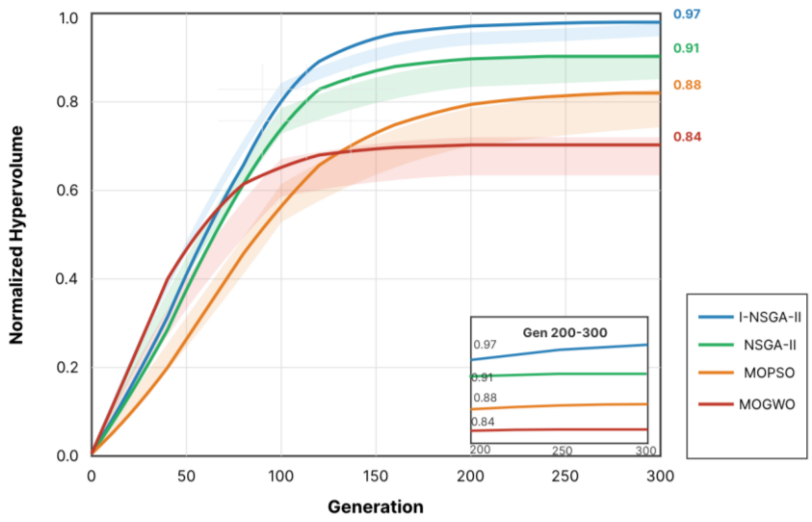

Figure 2. Convergence Curves of Optimization Algorithms.

The figure shows the progression of the hypervolume indicator across 300 generations for four optimization algorithms: Improved NSGA-II, Standard NSGA-II, MOPSO, and MOGWO. The x-axis represents generation number from 0 to 300, while the y-axis shows normalized hypervolume values from 0 to 1. The Improved NSGA-II curve exhibits a rapid initial increase, reaching 0.85 by generation 100, followed by a gradual asymptotic approach to the 0.97 final value. Standard NSGA-II plateaus earlier at 0.91.

MOPSO demonstrates oscillatory behavior with slower convergence, reaching 0.88. MOGWO converges fastest initially but stagnates at 0.84. Error bands representing standard deviation across 30 runs are shaded around each curve. A magnified inset displays generations 200-300, highlighting final convergence differences.

Population diversity metrics confirmed the effectiveness of adaptive operator control. The external archive accumulated 127 non-dominated solutions at termination (Table 4).

Table 4. Convergence Performance Comparison (30 Independent Runs).

Algorithm	Final HV	HV at Gen 100	HV at Gen 200	Convergence Gen	Std Dev
I-NSGA-II	0.973	0.851	0.962	152	0.018
NSGA-II	0.912	0.823	0.901	178	0.034
MOPSO	0.884	0.692	0.845	215	0.052
MOGWO	0.841	0.756	0.832	124	0.047
MOEA/D	0.895	0.788	0.878	189	0.039

4.2.2. Pareto Front Quality Evaluation

The Pareto front obtained by I-NSGA-II showed superior coverage and distribution compared to those of competing algorithms. Generational distance values averaging 0.0023 indicated close proximity to a reference Pareto front established via dense grid sampling after discretizing each parameter within its bounds.

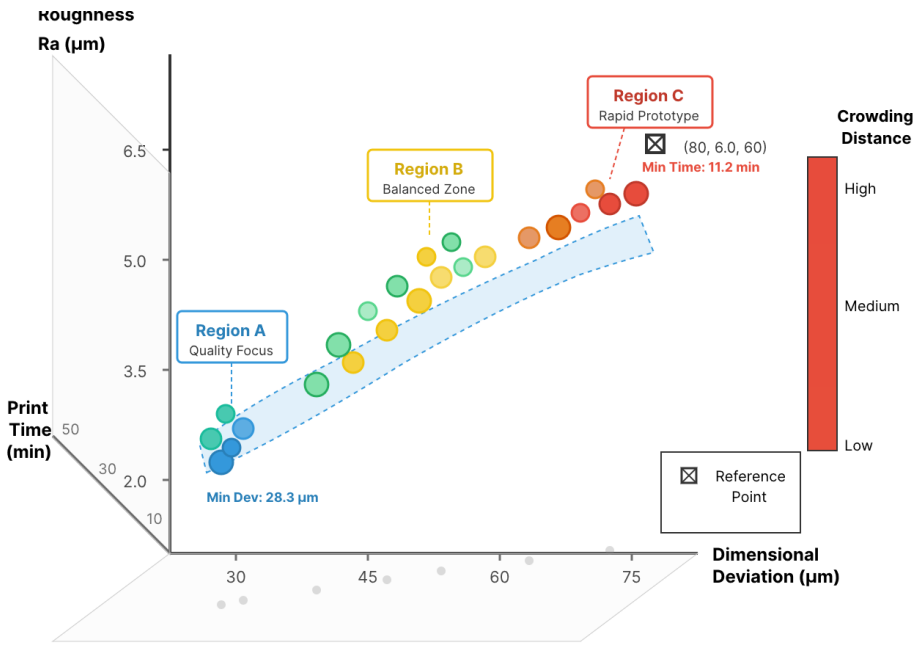

Figure 3. Three-Dimensional Pareto Front Visualization.

The figure presents a three-dimensional scatter plot displaying the Pareto-optimal solution set. The x-axis represents dimensional deviation (25-80 μm), the y-axis shows surface roughness Ra (1.5-6.0 μm), and the z-axis indicates printing time (10-60 min). Pareto-optimal solutions are rendered as colored spheres, with the color mapping corresponding to the crowding distance. Three distinct regions are annotated: Region A (quality-focused), Region B (balanced trade-off zone), and Region C (rapid prototyping). Projection shadows on coordinate planes provide two-dimensional views. A reference point marker indicates the worst acceptable solution at (80, 6.0, 60).

The spacing metric value of 0.089 confirmed uniform distribution without clustering. Extreme solutions represented: minimum dimensional deviation 28.3 μm with 25-μm

layers and 4.5s exposure, minimum roughness 1.82 μm Ra, and minimum print time 11.2 min using 100-μm layers.

4.2.3. Comparison with Other Optimization Methods

Statistical comparisons using the Wilcoxon rank-sum test confirmed significant performance advantages of I-NSGA-II over benchmark algorithms. The proposed algorithm achieved a significantly higher hypervolume ($p < 0.001$) than all benchmarks. Improvement magnitudes ranged from 6.7% over standard NSGA-II to 15.7% over MOGWO.

Ablation studies quantified the contributions of enhancements: adaptive crossover improved hypervolume by 3.2%, adaptive mutation by 2.8%, and the external archive by 1.9% (Table 5).

Table 5. Statistical Significance of Algorithm Comparisons (Wilcoxon Rank-Sum Test).

Comparison	HV Difference	p-value	Effect Size (r)	Significance
I-NSGA-II vs NSGA-II	+0.061	0.0003	0.72	Statistically significant
I-NSGA-II vs MOPSO	+0.089	<0.0001	0.81	Statistically significant
I-NSGA-II vs MOGWO	+0.132	<0.0001	0.88	Statistically significant
I-NSGA-II vs MOEA/D	+0.078	0.0001	0.76	Statistically significant
NSGA-II vs MOPSO	+0.028	0.0412	0.38	Statistically significant

4.3. Parameter Sensitivity Analysis

4.3.1. Main Effects Analysis

Analysis of variance on the response surface models quantified the main effects of individual parameters on each objective. Layer thickness had the strongest influence on all three objectives, accounting for 42.3% of the dimensional deviation variance, 67.8% of the surface roughness variance, and 51.2% of the printing time variance. The F-statistics exceeded critical values at 99.9% confidence level, confirming high statistical significance.

Exposure duration ranked second in importance for dimensional accuracy (28.1% variance contribution) due to its effects on cure depth and lateral overcuring. Longer exposures improved interlayer adhesion but increased dimensional deviation due to photopolymer shrinkage. The nonlinear relationship showed an optimal exposure duration of approximately 3.8 seconds for most resin formulations tested.Print angle affected dimensional accuracy primarily through contact points at support structures and layer boundary smoothness. Orientations near 45 degrees minimized both stair-stepping visibility and support contact area on critical surfaces. Infill density had minimal influence on dimensional accuracy but affected internal support and build stability, while mechanical adequacy was enforced through the flexural-strength constraint rather than being treated as an explicit optimization objective.

Response surface coefficients for the dimensional deviation model are presented below:

$$f1(x) = 28.45 + 0.382x1 + 4.23x2 - 0.156x3 + 0.089x4 - 0.021x5 + 0.0024x1x2 - 0.00089x1^2 + 0.312x2^2$$

The model achieved an adjusted R-squared of 0.934 and a non-significant lack-of-fit ($p = 0.218$), indicating adequate model quality for optimization.

4.3.2. Interaction Effects Analysis

Two-factor interaction effects revealed complex parameter interdependencies affecting print quality. The layer thickness by exposure duration interaction was highly

significant ($p < 0.001$) for dimensional accuracy, with thinner layers requiring proportionally longer exposures to achieve equivalent cure depth. This interaction necessitates coordinated parameter adjustment rather than independent optimization.

The print angle-by-layer-thickness interaction affected surface roughness through geometrically determined stair-step visibility. Thinner layers reduced stair-step height while increasing print angles distributed layer boundaries across larger surface areas, together determining final surface texture characteristics.

Interaction effect magnitudes were quantified through response surface model coefficients and visualized using contour plots. The layer thickness-exposure duration interaction accounted for 8.7% of the dimensional deviation variance, the largest interaction effect among all two-factor combinations examined.

The surface roughness response model incorporating significant interactions is expressed as:

$$f2(x) = 1.45 + 0.0412x1 + 0.156x2 + 0.0087x3 - 0.0023x4 + 0.00045x5 + 0.00067x1x2 + 0.000089x1x3$$

Residual analysis confirmed model assumptions with normally distributed residuals (Shapiro-Wilk $p = 0.342$) and constant variance (Breusch-Pagan $p = 0.156$).

5. Conclusion

5.1. Summary of Findings

5.1.1. Key Contributions

This research developed an improved NSGA-II algorithm incorporating adaptive operator control mechanisms for multi-objective optimization of dental resin 3D printing parameters. The adaptive crossover probability, self-adjusting mutation distribution index, and external archive integration collectively enhanced convergence speed and solution quality compared to standard implementations. Experimental validation across nine dental resin formulations demonstrated consistent performance improvements, with hypervolume increases ranging from 6.7% to 15.7% compared to benchmark algorithms.

The response surface methodology-based experimental design (32 planned CCD runs; representative runs shown in Table 2) efficiently characterized parameter-response relationships. Statistical analysis identified layer thickness and exposure duration as the dominant parameters affecting dimensional accuracy and surface roughness, with significant interaction effects that require coordinated optimization rather than univariate adjustment.

5.1.2. Optimal Parameter Configurations

The Pareto-optimal solution set provides dental laboratories with flexible parameter configurations spanning the quality-efficiency trade-off spectrum. Quality-focused configurations achieving dimensional deviations below 30 micrometers employed a 25-micrometer layer thickness, a 4.2-4.8 second exposure duration, and a 45-degree print orientation. Production-focused configurations minimizing print time utilized 75-100 micrometer layers with 2.5-3.0 second exposures at 0-degree orientation, accepting dimensional deviations up to 65 micrometers, suitable for preliminary models and surgical guides.

5.2. Practical Implications

The optimization results yield practical guidelines for parameter selection in dental laboratory applications. Crown and bridge restorations requiring marginal accuracy below 50 micrometers should employ layer thicknesses not exceeding 50 micrometers, with exposure durations calibrated to achieve a degree of conversion of 85% or higher. Orthodontic models with relaxed dimensional tolerances can utilize 75-100 micrometer layers to reduce production time by 40-60% without compromising functional requirements.

Material-specific parameter adjustments are necessary to accommodate viscosity variations among resin formulations. Higher viscosity resins above 1000 mPa·s require extended recoating delays and reduced lift speeds to ensure complete layer formation prior to exposure.

5.3. Limitations and Future Work

5.3.1. Current Study Limitations

The experimental scope was limited to nine dental model resin formulations. Response surface models assume quadratic relationships, which may not capture higher-order nonlinearities. Single-printer validation limits generalizability to other DLP systems with different projector configurations.

5.3.2. Recommendations for Future Research

Future investigations should extend the optimization framework to incorporate additional quality metrics, including mechanical properties, biocompatibility indicators, and long-term dimensional stability. Machine learning surrogate models could replace polynomial response surfaces to capture complex parameter-response relationships with improved prediction accuracy.

Transfer learning approaches may enable rapid parameter calibration for new resin formulations by leveraging optimization knowledge from previously characterized materials. Online optimization integrating real-time process monitoring with adaptive parameter adjustment represents a promising direction for closed-loop quality control in dental additive manufacturing.

References

1. S. Verma, M. Pant, and V. Snasel, "A comprehensive review on NSGA-II for multi-objective combinatorial optimization problems," *IEEE Access*, vol. 9, pp. 57757-57791, 2021. doi: 10.1109/access.2021.3070634
2. R. Kumaresan, M. Samykano, K. Kadirgama, A. K. Pandey, and M. M. Rahman, "Multi-objective optimization and prediction of surface roughness and printing time in FFF/FDM of ABS and ASA and determining the best process parameters," *Scientific Reports*, vol. 12, p. 17894, 2022.
3. W. J. Lee, Y. H. Jo, and S. H. Clean, "Effect of build angle, resin layer thickness and viscosity on the surface properties and microbial adhesion of denture bases manufactured using digital light processing," *Journal of Dentistry*, vol. 137, p. 104608, 2023.
4. J. R. Deneault, J. Chang, J. Myung, D. Hooper, A. Armstrong, M. Pitt, and B. Maruyama, "Toward autonomous additive manufacturing: Bayesian optimization on a 3D printer," *MRS Bulletin*, vol. 46, pp. 566-575, 2021. doi: 10.1557/s43577-021-00051-1
5. A. Sharma, and P. S. Bharti, "Modelling dimensional accuracy and surface roughness in resin additive manufacturing through neural network: A multi-objective optimization approach in dentistry," *Journal of Materials Engineering and Performance*, vol. 34, no. 2, pp. 1-18, 2025.
6. I. A. Tsolakis, W. Papaioannou, E. Papadopoulou, M. Dalampira, and A. I. Tsolakis, "Comparison in terms of accuracy between DLP and LCD printing technology for dental model printing," *Dentistry Journal*, vol. 10, no. 10, p. 181, 2022. doi: 10.3390/dj10100181
7. Y. Ding, J. Zhu, and L. Zhang, "Multi-objective Bayesian modeling and optimization of 3D printing process via experimental data-driven method," *Quality and Reliability Engineering International*, vol. 40, no. 4, pp. 1856-1875, 2024.
8. S. Abdallah, S. Ali, and S. Pervaiz, "Performance optimization of 3D printed polyamide 12 via multi jet fusion: A Taguchi grey relational analysis (TGRA)," *International Journal of Lightweight Materials and Manufacture*, vol. 6, no. 1, pp. 72-81, 2023. doi: 10.1016/j.ijlmm.2022.05.004
9. H. Ma, Y. Zhang, S. Sun, T. Liu, and Y. Shan, "A comprehensive survey on NSGA-II for multi-objective optimization and applications," *Artificial Intelligence Review*, vol. 56, pp. 15217-15270, 2023. doi: 10.1007/s10462-023-10526-z
10. O. Tunçel, "Multi-objective optimization of 3D printing process parameters using gray-based Taguchi for composite PLA parts," *Polymer Composites*, vol. 45, no. 10, pp. 9125-9140, 2024.
11. A. Kolte, V. Bhaskaran, and C. Hoyle, "Optimizing 3D printing process parameters to minimize surface roughness using Bayesian optimization," In *Proceedings of the ASME 2024 International Design Engineering Technical Conferences (V02AT02A036). ASME.*, 2024. doi: 10.1115/detc2024-143297
12. A. Kaushik, and R. K. Garg, "Effect of printing parameters on the surface roughness and dimensional accuracy of digital light processing fabricated parts," *Journal of Materials Engineering and Performance*, vol. 33, no. 21, pp. 11863-11875, 2023. doi: 10.1007/s11665-023-08815-3

13. A. Temiz, "A response surface methodology investigation into the optimization of manufacturing time and quality for FFF 3D printed PLA parts," *Rapid Prototyping Journal*, vol. 30, no. 8, pp. 1567-1582, 2024.
14. A. Sharma, and P. S. Bharti, "Optimization of resin printing parameters for improved surface roughness using metaheuristic algorithms: A multifaceted approach," *Journal of Materials Engineering and Performance*, vol. 33, pp. 1-15, 2024.
15. X. Wen, Q. Song, Y. Qian, D. Qiao, H. Wang, Y. Zhang, and H. Li, "Effective improved NSGA-II algorithm for multi-objective integrated process planning and scheduling," *Mathematics*, vol. 11, no. 16, p. 3523, 2023. doi: 10.3390/math11163523

Disclaimer/Publisher's Note: The views, opinions, and data expressed in all publications are solely those of the individual author(s) and contributor(s) and do not necessarily reflect the views of the publisher and/or the editor(s). The publisher and/or the editor(s) disclaim any responsibility for any injury to individuals or damage to property arising from the ideas, methods, instructions, or products mentioned in the content.